ON-LINE INTELLIGENT EVALUATION OF THE FATIGUE STATE OF A COMPOSITE CONVEYOR BELT

by

Xiuzhuang MEI[a,b,*]***, Changyun MIAO***[a,c*]***,***
Yanli YANG[c]***, and Xianguo LI***[c]

[a] School of Mechanical Engineering, Tianjin Polytechnic University, Tianjin, China
[b] School of Mechanical Engineering, Inner Mongolia University of Technology, Hohhot, China
[c] Tianjin Key Laboratory of Optoelectronic Detection Technology and System, Tianjin, China

Original scientific paper
https://doi.org/10.2298/TSCI200216105M

Fatigue failure of a composite conveyor belt occurs frequently, which will finally lead to an accident. An adaptive segmentation model is established to identify the rubber surface's fatigue failure and to evaluate the belt fatigue level by using the machine vision technology and the artificial bee colony algorithm. The results show that the damage rate of rubber surface can be correctly calculated and the fatigue failure state can be objectively evaluated.

Key words: *conveyor belt, fatigue failure, rubber surface damage rate, adaptive segmentation*

Instructions

Belt conveyors have become the main transportation equipment in various fields such as coal, mining, metallurgy, ports, electric power, building materials, and chemical industry. A composite material belt is composed of a base material and a core framework material, the former is generally rubber or plastic, while the latter includes metal, fabric and fiber. Composite belts often operate in a severe environment with dust and high humidity. Under the long-term effects of alternating mechanical stress, thermal oxidation, ozonation, *etc.*, the composite material is prone to fatigue failure. Severe fatigue failure can weaken the toughness and reduce the tensile strength of composite materials. If the fatigue failure is not repaired in a timely manner, accidents such as longitudinal tearing and lateral breakage of conveyor belts will occur, causing personal injury and huge economic loss. For the sake of simplification, this study uses conveyor belt to represent composite conveyor belt.

The belt fatigue failure is mainly characterized by rubber surface breakage in forms of crack and holes. Currently, most users adopt the ocular estimate to detect the breakage of the belt bearing surface under low-speed and no-load conditions. As a result, the non-bearing surface can hardly be visually inspected. The detection quality is determined by the responsibilities and professional skills of the technicians, as a result, the evaluation quality of belt fatigue state can be hardly guaranteed.

* Corresponding authors, e-mail: 120681916@qq.com; miaochangyun1962@sina.com

At present, many scholars had carried out in-depth research on fatigue performance and fatigue damage of composite materials, and proposed various mathematical models and detection methods for fatigue analysis and life prediction. Yan *et al.* [1] determined fatigue damage state by a ultrasonic guided waves method. Marcantonio *et al.* [2] described the feasibility of non-linear ultrasonic waves in the detection of materials evaluation in fatigue, thermal and corrosion damage. Shabani *et al.* [3] put forward a reliable prediction for fatigue life of the unidirectional e-glass/epoxy composite plies by using progressive fatigue damage models. The research on the technology of monitoring belt fatigue state mainly focuses on aspects such as damage mechanism and experimental analysis of splice fatigue strength. Andrejiova *et al.* [4] investigated the influence of belt carcass structure, impact height, and impactor type on the damage degree of conveyor belts. Kirjanow-Blazej *et al.* [5] carried out an electromagnetic testing to detect wire rope core damage in an attempt to predict the belt residual life by employing the linear regression model. Bajda *et al.* [6] analyzed the effects of belt length and joint number change on the conveyor belt durability. Kozlowski *et al.* [7] analyzed the changes in technical conditions such as joint length and joint center bias by using the magnetic method to monitor the joint. Li *et al.* [8] examined the relationship between joint deformation and strength based on the finite element simulation analysis. Hao *et al.* [9] applied visual saliency to identify belt rubber surface scratch. Research on belt fatigue state monitoring is mostly at the theoretical and laboratory stage. Therefore, to apply it in practical engineering, numerous key technical problems remain to be solved.

In this study, an adaptive segmentation model of belt images is established based on the image acquisition characteristics of linear array camera. The artificial bee colony algorithm is used to calculate the adaptive segmentation parameters and realize image segmentation under the coupling effects of multiple environmental factors, thus effectively suppressing the interference such as uneven illumination, rubber surface scratches and water spots. Finally, the deep belief network is employed to classify, identify and analyze the fatigue failure on rubber surface of conveyor belts. The fatigue state of the conveyor belts is evaluated reasonably according to the proposed value of the damage rate parameter, which provides a theoretical basis for maintenance and life prediction of conveyor belts.

Image acquisition device

The rubber surface of the conveyor belt includes the bearing surface and the non-bearing surface. In order to obtain the complete information about rubber surface, this study uses two image acquisition devices. The first collection device is installed between the upper and lower belt to collect the information about the non-bearing surface. Three linear LED light sources and a linear array CCD camera with 2048 px and a maximum line frequency of 19 kHz are used. The structural arrangement is shown in fig. 1. The linear light source 2 is placed transversely, and the linear light sources 1 and 3 are placed obliquely. The position is generally similar to the arc shape of the conveyor belt. The second set of acquisition device is installed below the conveyor belt and a long linear LED light source is used. The camera type is the same as the first acquisition device.

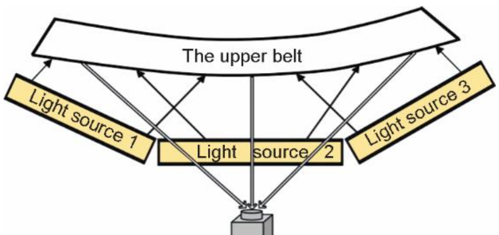

Figure 1. Image acquisition devices for monitoring the non-bearing surface

Adaptive segmentation algorithm of belt image

The belt image is represented as $I(i, j)$, $i < H$ and $j < W$, where H is the image height, and W is the image width. The image width direction is consistent with the conveyor width direction, and the image height direction is along the operation direction of the conveyor belt. The linear array camera and the light sources are fixed on the image acquisition device of the conveyor belt. The same acquisition unit of the linear array camera receives the same light at different time. Based on this feature, a conveyor image segmentation model is established. The model output $I_o(i, j)$ is:

$$I_o(i,j) = 0.5 - 0.5\text{sign}[I(i,j) - k_1 M(j) - k_2 R_{\text{mse}} F(j) + k_3 V_{\min} + \varepsilon] \tag{1}$$

where k_1, k_2, and k_3 are adjustment coefficients. The k_1 and k_2 belong to [0, 1], and k_3 belongs to [0, 10], $V_{\min}$ – the minimum gray value of all pixels, and ε – the minimum value greater than zero. In addition:

$$M(j) = \frac{1}{H}\sum_{i=1}^{H} I(i,j), \quad j = 1,2,3,\cdots,W \tag{2}$$

$$R_{\text{mse}} = \sqrt{\frac{1}{W}\sum_{j=1}^{W}[\mathrm{M}(j) - \frac{1}{W}\sum_{j=1}^{W}\mathrm{M}(j)]^2} \tag{3}$$

$$\mathrm{F}(j) = \text{sign}\left\{\frac{1}{H}\sum_{i=1}^{H}[\mathrm{I}(i,j) - \mathrm{M}(j)]^2\right\} \tag{4}$$

where $M(j)$ is the average value of pixels in column j, R_{mse} – the mean squared error in image horizontal direction, and $F(j)$ – the flag of image foreground. When light distribution is uneven, k_1 is greater. The stronger the line-direction noise, the greater the value of k_2, the stronger the light reflected on the rubber surface, the larger the value of k_3.

To solve the adjustment coefficients k_1, k_2, and k_3, the objective function is established:

$$O(I_o) = A(I_o) + \frac{0.7}{H \times W}\sqrt{\sum_{i=1}^{H}\sum_{j=1}^{W}[H \times W \times I_o(i,j) - A(I_o)]} + \frac{10}{E(I_o)} \tag{5}$$

where

$$A(I_o) = \sum_{i=1}^{H}\sum_{j=1}^{W} I_o(i,j)$$

which is the image area:

$$E(I_o) = -\sum_{n=0}^{255} p_n \log_2 p_n$$

which is the 1-D entropy, p_n is the probability that the gray value n appears.

Finally, with eq. (5) as the objective function, the artificial bee colony algorithm [10] is used to obtain the adjustment coefficient of the segmentation model of eq. (1). There are a total of 40 colonies and 20 nectar sources. The maximum number of iterations and updates are both 10.

The segmentation effect is analyzed by taking the image with uneven illumination and without damage, longitudinal crack image, transverse crack image at surface scar, the image of the holes on the aging rubber surface, and the damaged image with water spots, as shown in fig. 2.

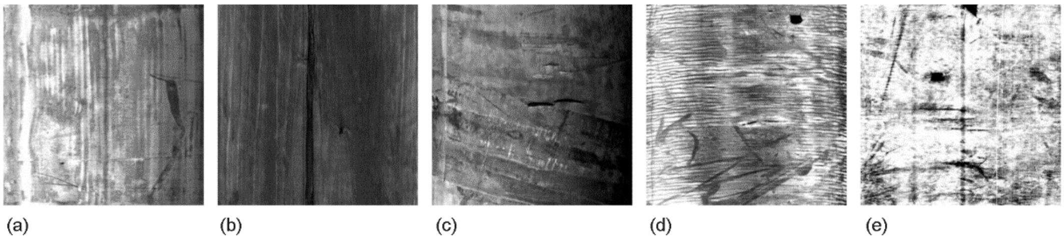

Figure 2. Examples of image segmentation; (a) irregular light without damage, (b) longitudinal crack, (c) transverse cracks at surface scar, (d) holes on aged rubber surface, and (e) damage with water spots

In image segmentation, the parameters of k_1, k_2, and k_3 are calculated by using the artificial bee colony algorithm, as shown in tab. 1. Every segmentation parameter changes under different environmental backgrounds or different interferences. If the light sources in fig. 2(a) are stronger, the value of k_1 is larger. If the line interference in figs. 2(a)-2(d) is stronger, the value of k_2 is larger. Figure 2(d) shows the aging rubber material and fig. 2(e) is the noise with water spots. The larger value of k_3 indicates the better environmental adaptability of the segmentation algorithm.

Table 1. Optimization parameter value table

Figure number	k_1	k_2	k_3
Figure 2(a)	0.52	1.00	0.40
Figure 2(b)	0.15	1.00	0.36
Figure 2(c)	0.08	0.13	0.10
Figure 2(d)	0.10	0.72	1.00
Figure 2(e)	0.09	0.31	0.95

Finally, the segmentation parameters are used for image segmentation. The image segmentation results are shown in fig. 3. The light on the left side of fig. 2(a) is bright and the illumination is uneven. After image segmentation, the influence of uneven illumination is suppressed in fig. 3(a). However, there are some isolated points and a small part of noise, which can be filtered by simple filtering. Figure 2(b) is an image of a longitudinal crack with uneven illumination. After segmentation, there is noise in fig. 3(b), which should be filtered subsequently. Figure 2(c) shows transverse cracks at surface scar. After segmentation, the influence of surface scar is suppressed in fig. 3(c). Figure 2(d) is an image of damage on the aging rubber surface with tiny aging cracks and uneven illumination. The effects of aging cracks and uneven illumination are suppressed after segmentation in fig. 3(d), and the segmentation effect is good. Figure 2(e) is an image of damage with water spots and slight scratches, and the segmentation result in fig. 3(e) is not affected. The adaptive algorithm for belt image based on the artificial bee colony has good segmentation effect and strong anti-noise capacity. It can suppress noise interference such as uneven lighting, water spots, slight scratches, surface scar, and aging rubber surface.

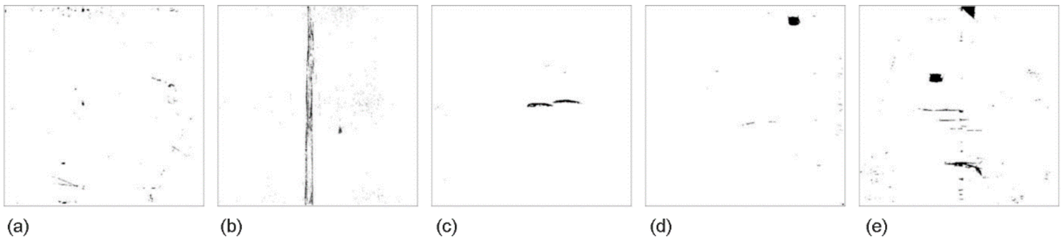

Figure 3. The segmentation results of figs. 2(a)-2(c)

Classification and identification of fatigue failure on belt rubber surface

After adaptive segmentation of belt image, small-area image noise can be filtered through morphological processing, and the fatigue failure on rubber surface of the conveyor belts can be classified and identified. The fatigue failure is divided into longitudinal cracks, transverse cracks and non-linear damage. Longitudinal cracks and transverse cracks refer to longitudinal and transverse defects resulted from local cracking caused by factors such as deep scratches and rubber surface aging. Other forms of fatigue failure include non-linear damage, including holes, bumps, peeling, *etc.* The examples of damage on the rubber surface of transverse cracks, longitudinal cracks, and holes are shown in fig. 4. The image resolution is 256 px × 256 px. The nylon fabric core in the most severely damaged crack is exposed in fig. 4(b).

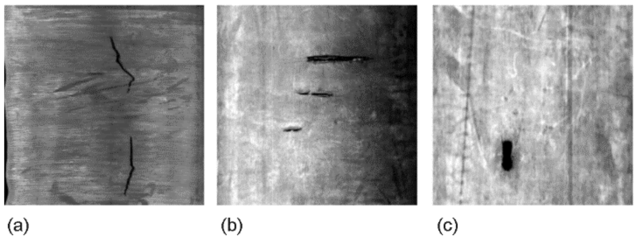

Figure 4. Classification of fatigue failure on rubber surface; (a) longitudinal cracks, (b) transverse cracks, and (c) holes

Figure 4 was conducted with adaptive image segmentation, and the image noise with an area smaller than 600 px^2 was filtered. The processing result of fig. 4 is shown in fig. 5, where c_1~c_7 are damage numbers. For figs. 5(a)-(c), We firstly calculate the image dispersion, D_s, elongation, E_s, rectangularity, R_s, main direction angle, β, and 1-D Fourier descriptors, $F_d(u)$. The vectors respectively expressed:

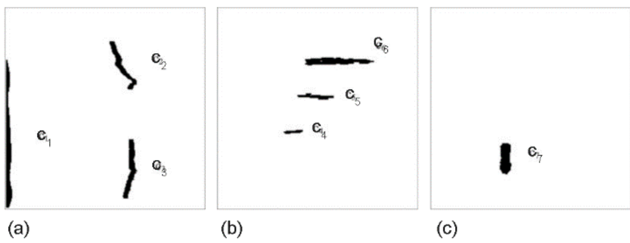

Figure 5. The processing results of figs. 4(a)-4(c)

$$D_s = 4\pi \frac{A_s}{L_s^2} \tag{6}$$

$$E_s = \frac{A_s}{W_s^2} \tag{7}$$

$$R_s = \frac{A_s}{A_r} \tag{8}$$

$$\beta = \begin{cases} \alpha + \pi, & \text{when } \mu_{3,0} > 0 \\ \alpha, & \text{others} \end{cases} \tag{9}$$

$$F_d(u) = \frac{|d(u+1)|}{|d(1)|}, \quad u = 2, 4 \tag{10}$$

where A_s is the damaged area, L_s – the perimeter of the damaged contour, W_s – the maximum width of the damage, and A_r – the smallest circumscribed rectangular area. In addition:

$$\alpha = \arctan\left[\frac{\mu_{0,2} - \mu_{2,0} + \sqrt{(\mu_{0,2} - \mu_{2,0})^2 + 4\mu_{1,1}{}^2}}{2\mu_{1,1}}\right] \tag{11}$$

where $\mu_{0,2}$, $\mu_{2,0}$, $\mu_{1,1}$, and $\mu_{3,0}$ are the $p + q$ order center moment of the damaged area. Equation (12) is 1-D Fourier descriptor expressing N number boundary points $x(n) + jy(n), n = 1, \cdots, N$:

$$d(u) = \frac{1}{N}\sum_{n=0}^{N-1}[x(n) + jy(n)]e^{-j2\pi un/N} \tag{12}$$

The feature information of surface damage is shown in tab. 2. Non-linear damage has the dispersion value greater than 0.85, elongation degree smaller than 1.5 and rectangularity degree greater than 0.9, and $F_d(4)$ is 1. The $F_d(2)$ of transverse and longitudinal cracks is 1. The main direction angles of the longitudinal and the transverse cracks are close to 90° and 0°, respectively. It can be seen that the selection of the feature vector is accurate and effective.

The deep belief network was used to classify and identify the damage on the rubber surface of the conveyor belts. The 500 training samples and 300 test samples were used for each type of damage, and the training samples and test samples were not repetitive. The recognition accuracy of non-linear damage, transverse and longitudinal crack is 95.3%, 98.5%, and 99.5%, respectively. Therefore, the accuracy of belt damage classification is more than 95%, which meets the requirements of engineering.

Table 2. Feature information of surface damage in fig. 5

Damage number	D_s	E_s	R_s	β	$F_d(2)$	$F_d(4)$
c_1	0.227	8.798	0.832	89.315	1	0.093
c_2	0.647	1.844	0.556	64.058	1	0.224
c_3	0.617	1.849	0.720	84.010	1	0.371
c_4	0.842	1.703	0.889	3.719	1	0.111
c_5	0.713	2.246	0.859	2.895	1	0.309
c_6	0.571	3.356	0.885	0.261	1	0.141
c_7	0.919	1.309	0.907	89.340	0.085	1

Evaluation of fatigue state of conveyor belts

In this study, the fatigue state of the conveyor belts is evaluated according to the damage rate on rubber surface, which is defined as variable R_d. A total number of N images is acquired in the rotation period. The belt in the image has the width W_b and the height H_b. The parameter, R_d , is defined as:

$$R_d = \left(\frac{0.4A_n}{N \times H_b \times W_b} + \frac{0.5L_l}{N \times H_b} + \frac{0.1L_t}{N \times W_b} \right) 100\% \tag{13}$$

where A_n, L_l, and L_t are the total area of non-linear damage, the total length of longitudinal cracks, and the total length of transverse cracks of the entire conveyor belt.

After confirmation by many managers in charge of the conveyor belts, the fatigue state of the conveyor belt is divided into three grades of *good*, *medium,* and *poor*. When R_d is less than 10%, the grade is *good*, which means that the conveyor belt has no fatigue or slight fatigue, and can be used normally with regular maintenance. When R_d is greater than or equal to 10% and less than 20%, the grade is *medium*, which indicates that the conveyor belt is fatigued and requires comprehensive maintenance. When R_d is greater than or equal to 20%, the grade is *poor*, which means that the conveyor belt is severely fatigued and recommended to be scrapped.

A laboratory-made belt conveyor is tested to verify the effectiveness of the above method. The roller diameter of the conveyor is 0.52 m. The belt size is 10 m × 0.65 m and its core material is nylon fabric. The test results are shown in tab. 3, where S_r is the running speed of conveyor belt and F_l is the line frequency of linear array camera in tab. 3. The actual resolution of surface damage of conveyor belt is 0.78 mm × 0.78 mm. The values of A_n, L_l, L_t and R_d are different slightly at different operating speeds, which is not affected by the running speed, showing that the robustness is good.

Table 3. Examples of rubber surface damage rate

S_r [ms^{-1}]	F_l [Hz]	H_b [px]	W_b [px]	A_n [px^2]	L_l [px]	L_t [px]	R_d
0.25	320	1024	1040	24736	2384	1594	11.07%
0.5	640	1024	1045	16458	2333	1820	11.57%
1	1280	1024	1045	30222	2246	1592	11.56%

The proposed algorithm was used to detect the fatigue state of 60 conveyor belts in 2 docks, 4 coal mines, and 3 thermal power plants. The evaluation accuracy rate of the fatigue level of the conveyor belts is up to 100%.

Conclusions

The present study investigated an on-line intelligent evaluation method for the fatigue state of composite material conveyor belts. Additionally, an image adaptive segmentation algorithm is proposed, which effectively suppresses the coupled noise influences such as mechanical scratch, sticking substance and water spots, as well as the uneven illumination on rubber surface. Besides, the classification and recognition algorithm of belt rubber surface breakage is also proposed, achieving the accurate recognition rate of over 95%. The model for calculating the damage rate of rubber surface is established, realizing the evaluation of belt fatigue level with the accurate evaluation rate of 100%. According to the experimental results, the method proposed in the current work can be used in on-line evaluation of belt fatigue state, also providing reliable objective evidence for maintenance and life prediction of conveyor belts.

Acknowledgment

This work was financially supported by the Key Program of Natural Science Foundation of Tianjin, China (No. 17JCZDJC31600), the Key Program of Science and Technology Support Plan of Tianjin (No. 18YFZCGX00930), and the Tianjin Result Transformation Support Key R & D Project (No. 18YFJLCG00060). The authors express gratitude to anonymous reviewers for their comments on the manuscript.

References

[1] Yan, G., *et al.*, Guided Wave-Based Monitoring of Evolution of Fatigue Damage in Glass Fiber/Epoxy Composites, *Applied Sciences, 9* (2019), 7, pp. 1394-1410
[2] Marcantonio, V., *et al.*, Ultrasonic waves for Materials Evaluation in Fatigue, Thermal and Corrosion Damage: A Review, *Sciences Mechanical Systems and Signal Processing, 120* (2019), Apr., pp. 32-42
[3] Shabani, P., *et al.*, Life Prediction of a Notched Composite Ring Using Progressive Fatigue Damage Models, *Composites Part B: Engineering, 165* (2019), May, pp. 754-763
[4] Andrejiova, M., *et al.*, Failure Analysis of the Rubber-Textile Conveyor Belts Using Classification Models, *Engineering Failure Analysis, 101* (2019), July, pp. 407-417
[5] Kirjanow-Blazej, A., *et al.*, Forecast of the Remaining Lifetime of Steel Cord Conveyor Belts Based on Regression Methods in Damage Analysis Identified by Subsequent DiagBelt Scans, *Engineering Failure Analysis, 100* (2019), June, pp. 119-126
[6] Bajda, M., *et al.*, Analysis of Changes in the Length of Belt Sections and the Number of Splices in the Belt Loops on Conveyors in an Underground Mine, *Engineering Failure Analysis, 101* (2019), July, pp. 436-446
[7] Kozlowski, T., *et al.*, Magnetic Methods in Monitoring Changes of the Technical Condition of Splices in Steel Cord Conveyor Belts, *Engineering Failure Analysis, 104* (2019), Oct., pp. 462-470
[8] Li, X. G., *et al.*, Influence of Different Cord Pitch on the Pullout Force of Steel Cord Conveyor Belt Splice, *Journal of Adhesion Science and Technology, 32* (2018), 20, pp. 2268-2281
[9] Hao, X. L., *et al.*, A Multi-Class Support Vector Machine Real-Time Detection System for Surface Damage of Conveyor Belts Based on Visual Saliency, *Measurement, 146* (2019), Nov., pp. 125-132
[10] He, Z. Z., *et al.*, Determination of Aerosol Particle Size Distribution by a Novel Artificial Bee Colony-Differential Evolution Hybrid Algorithm, *Thermal Science, 23* (2019), 2B, pp. 1161-1172

Paper submitted: February 16, 2020
Paper revised: July 4, 2020
Paper accepted: July 4, 2020